Laser Cutting of Rectangular Blanks in Thick Sheet Steel: Effect of Cutting Speed on Thermal Stresses

B.S. Yilbas, A.F.M. Arif, and B.J. Abdul Aleem

Laser cutting of rectangular blank in thick sheet steel is considered and temperature as well as stress fields in the cutting section are predicted using the finite element method. The influence of cutting speed on temperature and stress levels is examined while the XRD technique is introduced to measure the residual stresses after the laser cutting process. The morphological and metallurgical changes in the cutting section are examined using the SEM and XRD. Microhardness across the cut cross section is measured. It is found that the temperature gradient along the y-axis changes, which modifies von Mises stress distribution along the y-axis. The residual stress predicted agrees with the measured data for all the cutting speeds employed in the present study.

1. Introduction

Laser machining has several advantages over the conventional machining processes due to the short processing time precision of operation, local thermal affects, and acceptably good end product quality. Laser cutting is one of the widely used laser machining processes in industry. However, when cutting high aspect ratio (length to width) parts in thick sheet metals, thermal stress developed around the cut edges becomes important, particularly in the corners of the rectangular shapes. Controlling the cutting speeds in such cutting situation may improve the stress levels around the cut edges. Consequently, investigation into laser cutting of high aspect ratio rectangular shapes in thick sheet metal and influence of cutting speeds on the resulting stress fields becomes essential.

Considerable research studies are carried out to examine the laser cutting process and thermal stress development. Li and Sheng (Ref 1) investigated stress developed during laser cutting of ceramics using the plane stress model. They analyzed the fracture initiation quantitatively and indicated that the surface fracture occurred at high intensity irradiation. The intensity factor for semi-infinite crack formed by a moving thermal source was examined by Kotousov (Ref 2). They developed analytical solution for the stress intensity factor in the tip of the cut. The thermal stress development during laser treatment of ceramics was investigated by Modest and Mallison (Ref 3). The analysis adopted covered three pulse and continuous modes of heating and they indicated that tensile stress was developed over a thick layer below the surface. Thermo-mechanical modeling of laser cutting was carried out by Hardjadinata and

Doumanidis (Ref 4). They used a flexible thermo-mechanical finite element model to determine the layer deformation due to the thermal gradients. Laser cutting of ceramics and thermal stress development were examined by Tsai and Chen (Ref 5). They obtained the relationship between stress levels, laser power, cutting speed, and specimen geometry. A probabilistic model for the crack formation in laser cutting of ceramics was introduced by Lee and Ahn (Ref 6). They used a Bayesian model for crack formation over a thin aluminum plates during the laser cutting process. The propagation of crack tip during

Nomenclature	
a	beam diameter at the surface, m
C_p	Specific heat capacity, J/kg K
$[K]$	element stiffness matrix
$\{F^{th}\}$	elemental thermal load vector
$\{F^{pr}\}$	elemental pressure vector
$\{F^n\}$	nodal force vector
k	thermal conductivity, W/m K
p	load vector, N
$[N_s]^T$	shape matrix
T	temperature, K
T_o	initial temperature, K
t	time, s
u	laser cutting speed, m/s
δU	strain energy, J
$\{\delta u\}^T$	vector for virtual displacements
δV	external work, J
w	workpiece thickness, m
x, y, z	space coordinates

Greek Symbol	
$\{\alpha\}$	vector of coefficients of thermal expansion
$\{\varepsilon^{th}\}$	thermal strain vector
δ	absorption coefficient, 1/m
υ	Poisson's ratio
ρ	density, kg/m^3

B.S. Yilbas, A.F.M. Arif, and **B.J. Abdul Aleem**, ME Department, KFUPM, Dhahran, Saudi Arabia. Contact e-mail: bsyilbas@kfupm. edu.sa.

the laser cutting of glass sheets was investigated by Paterson et al. (Ref 7). They showed that stress levels were high in the immediate vicinity of the crack tip and heating/cooling loading conditions were favorable for straight line cutting. The thermal stress distribution and failure mode analysis for laser cutting process were examined by Akarapu et al. (Ref 8). They showed that the groove shapes as well as the temperature and stress distributions were similar in front of the cutting section. Thermal stress analysis during laser treatment of cemented carbide cutting tool was carried out by Yilbas et al. (Ref 9). They indicated that multidirectional cracks were formed at the surface and tungsten nitride was formed in the surface region after the laser treatment process. Thermo-mechanical effect during laser assisted machining was examined by Germain et al. (Ref 10). They indicated that the diffusion in the machined section reduced the residual stress levels in the workpiece. Thermal stress development during laser heating process was examined by Yilbas and Al-Ageeli (Ref 11-14). They developed analytical solution for temperature and stress fields; however, the formulation was limited to the one-dimensional heating situation.

Arif and Yilbas (Ref 15) investigated thermal stress development during laser cutting of steel. They showed that the high stress levels were developed in the vicinity of the cut edges. However, the study was limited with the thin sheet metal cutting applications and the modeling for thermal stress development due to corner cutting was not considered. Consequently, in the present study, thermal stress field developed during laser cutting of high aspect ratio (length-to-width ratio) rectangular blank in thick sheet metal is considered. Temperature and stress fields in the cutting sections are computed using the finite element model. The laser cutting experiment is carried out using the identical cutting conditions adopted in the simulations. The residual stress developed in the cutting section is measured using the XRD technique. The results are, then, compared with the predictions. The morphological and metallurgical changes in the cutting sections are examined via SEM. The experiment and simulations are repeated for three laser cutting speeds. A mild steel sheet with 5 mm thickness is used as a workpiece.

2. Heat Transfer Analysis

The transient diffusion equation based on the Fourier heating model can be written in the Cartesian coordinates as:

$$\rho\frac{\partial(C_pT)}{\partial t} = \left(\frac{\partial}{\partial x}\left(k\frac{\partial T}{\partial x}\right)+\frac{\partial}{\partial y}\left(k\frac{\partial T}{\partial y}\right)+\frac{\partial}{\partial z}\left(k\frac{\partial T}{\partial z}\right)\right)+\rho u\frac{\partial(C_pT)}{\partial y}$$

(Eq 1)

where x, y, and z are the axes (Fig. 1), u is the scanning speed of the laser beam, ρ is the density, C_p is the specific heat capacity, and k is the thermal. It should be noted that the laser heating situation is considered to be a constant temperature line heat source with a radius a (laser beam radius at focused surface) in the x-y plane and a thickness w along the z-axis. This setting represents the situation that at the kerf surface temperature is assumed to be at melting temperature of the substrate material along the z-axis in the x-y plane where laser beam is located (Fig. 1).

At the free surface (in x-y plane at $z = 0$), a convective boundary is assumed, therefore, the corresponding boundary condition is:

At $z = 0$ (at the surface) $\rightarrow \dfrac{\partial T}{\partial z} = \dfrac{h}{k}(T_s - T_o)$

where h is the heat transfer coefficient and T_s and T_o are the surface and reference temperatures, respectively. In addition, at a distance far away from the surface in the x-y plane temperature becomes the same as the reference temperature. This yields the boundary condition of:

At x and $y = \infty \rightarrow T = T_o$ ($T_o = 300$ K)

Initially, the substrate material is assumed to be at a reference temperature (T_o), therefore, the initial condition becomes:

At $t = 0 \rightarrow T = T_o$ ($T_o = 300$ K)

3. Modeling of Thermal Stresses

From the principle of virtual work (PVW), a virtual (very small) change of the internal strain energy (δU) must be offset by an identical change in external work due to the applied loads (δV). Considering the strain energy due to thermal stresses resulting from the constrained motion of a body during a temperature change, PVW yields:

$$\{\delta u\}^T \int_{\text{vol}} [B]^T[D][B]dv\{u\} - \{\delta u\}^T \int_{\text{vol}} [B]^T[D]\{\varepsilon^{th}\}dv$$
$$= \{\delta u\}^T \int_{\text{Area}} [N_s]^T\{p\}dS + \{\delta u\}^T\{F_N\}$$

(Eq 2)

Noting that the $\{\delta u\}^T$ vector is a set of arbitrary virtual displacements common in all of the above terms, the condition required to satisfy above equation reduces to:

$$[K]\{u\} = \{F^{th}\} + \{F^{pr}\} + \{F^n\}$$

(Eq 3)

where

$[K] = \int_{\text{vol}} [B]^T[D][B]dv = $ element stiffness matrix

$\{F^{th}\} = \int_{\text{vol}} [B]^T[D][\varepsilon^{th}]dv = $ element thermal load vector

$\{\varepsilon^{th}\} = \{\alpha\}\Delta T = $ thermal strain vector

$\{\alpha\} = $ vector of coefficients of thermal expansion

$\{F^{pr}\} = \int_{\text{Area}} [N_s]^T\{p\}dS = $ element pressure vector

$\{F^n\} = $ nodal force vector

In the present study, the effect of mechanical deformation on heat flow has been ignored and the thermo-mechanical phenomenon of melting is idealized as a sequentially coupled unidirectional problem. For thermal analysis, the given structure is modeled using thermal element (SOLID70). SOLID70 has a 3D thermal conduction capability (ANSYS code). The element has eight nodes with a single degree of freedom, temperature, at each node. The element is applicable to a 3D, steady-state or transient thermal analysis. Since the model containing the conducting solid element is also to be analyzed structurally, the element is replaced by an equivalent structural element (such as SOLID45) for the structural analysis.
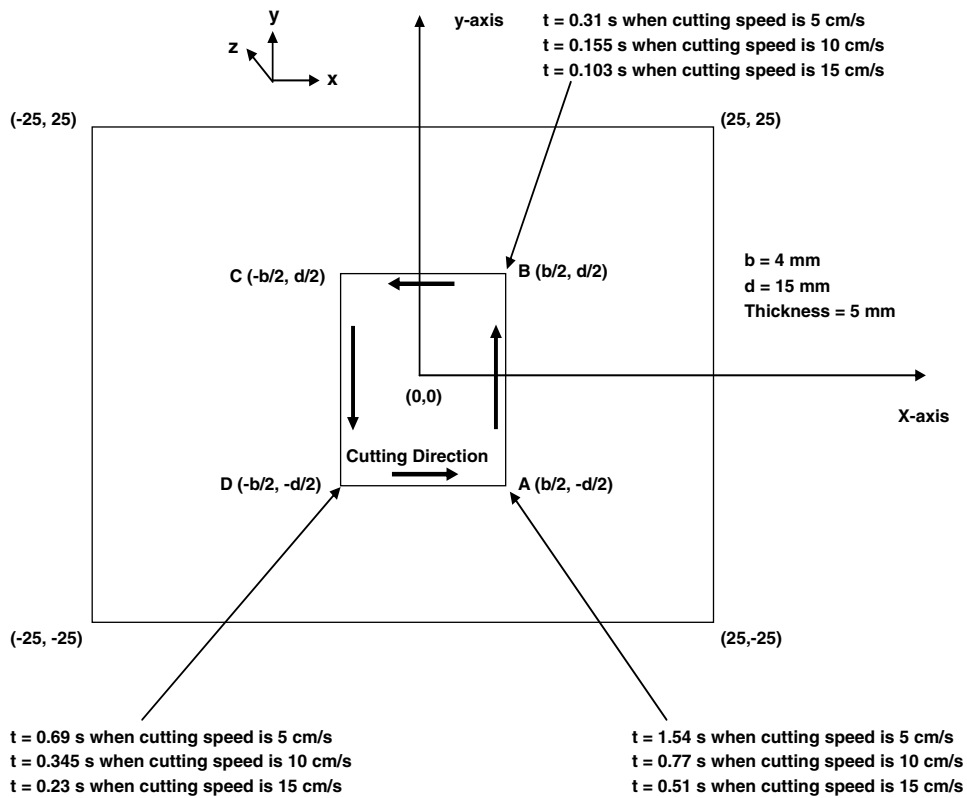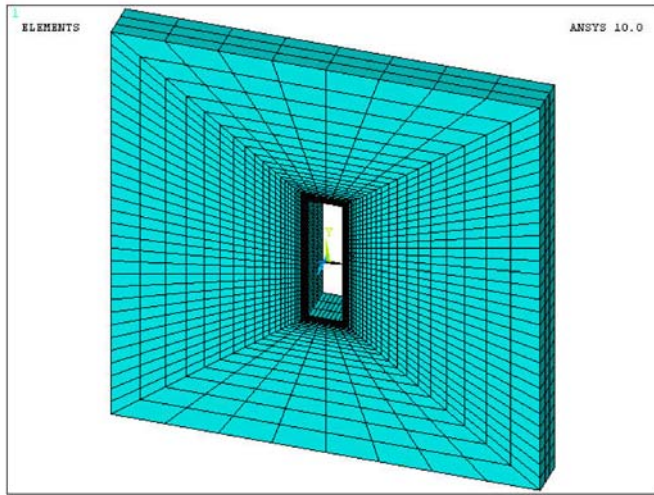
Fig. 1 Geometric arrangements of the cut square cutting

SOLID45 is used for the 3D modeling of solid structures. The element is defined by eight nodes having three degrees of freedom at each node: translations in the nodal x, y, and z directions. The element has plasticity, creep, swelling, stress stiffening, large deflection, and large strain capabilities.

The thermal and mechanical properties used in the simulations are given in Table 1.

4. Experimental

The laser used in the experiment is a CO_2 laser (LC-αIII-Amada) and delivering nominal output power of 2000 W at the

Table 1 Mechanical and thermal properties of the mild steel used in the simulations

Temperature, K				373
$\alpha \times 10^{-6}$, 1/K				63
υ				0.29
E, GPa				210
ρ, kg/m^3				7854

	Temperature, K				
	300	**400**	**600**	**800**	**1000**
k, W/m K	60.5	56.7	48	39.2	30
C_P, J/kg K	434	487	559	685	1169

pulse mode with adjustable frequencies. Nitrogen emerging from a conical nozzle and co-axially with the laser beam is used. The 127 mm focal lens is used to focus the laser beam. The laser cutting parameters are given in Table 2.

JEOL JDX-3530 scanning electron microscope (SEM) is used to obtain photomicrographs of the cross section and surface of the workpieces after the tests. The Bruker D8 Advance having Mo$K\alpha$ radiation is used for XRD analysis. A typical setting of XRD was 40 kV and 30 mA. It should be noted that the residual stress measured using the XRD technique provides the data in the surface region of the specimens. This is because of the penetration depth of Mo-$K\alpha$ radiation into the coating, i.e., the penetration depth is in the order of 10-20 μm. The measurement relies on the stresses in fine-grained polycrystalline structure. The position of the diffraction peak undergoes shifting as the specimen is rotated by an angle ψ. The magnitude of the shift is related to the magnitude of the residual stress. The relationship between the peak shift and the residual stress (σ) is given (Ref 16):

$$\sigma = \frac{E}{(1 + \upsilon)\mathrm{Sin}^2\psi} \frac{(d_n - d_o)}{d_o} \qquad \text{(Eq 4)}$$

where E is Young's modulus, υ is Poisson's ratio, ψ is the tilt angle, and d_n are the d spacing measured at each tilt angle. If there are no shear strains present in the specimen, the d spacing changes linearly with $\sin^2\psi$.

The square envelope was cut in 15×4 mm^2, as shown in Fig. 1, from a steel sheet with 5 mm thickness. The sheet metal was cleaned chemically prior to laser cutting process.

5. Results and Discussion

Laser cutting of rectangular blanks in mild sheet metal is considered and the influence of cutting speed on temperature and thermal stress fields is examined. Finite element method (FEM) is used to predict temperature and stress fields in the cutting regions while the XRD technique is introduced to measure the residual stress developed after the cutting process.

Figure 2 shows temperature variation along the y-axis at two locations at the cut surface (Fig. 1) for three different cutting speeds while Fig. 3 shows the plane view of temperature distribution around the cut edges. It should be noted that the coordinates of the first location $x = -2.75$ mm, $y = 7.5$ mm, and $z = 0$ mm is the region very close to the point "D" as shown in Fig. 1 while $x = -2.75$ mm, $y = -7.5$ mm, and $z = 0$ mm is the region very close to the point "A" as shown in Fig. 1. Since the laser cutting speed is different, time taken to reach points A and B are different for the each speed. Temperature attains high value in the region close to the maximum laser power intensity. Temperature decays sharply from its maximum along the y-axis; however, temperature decay becomes gradual as the distance from the laser source increases further along the y-axis. This situation is true at location $x = -2.75$ mm, $y = 7.5$ mm, and $z = 0$ mm. The

influence of laser scanning velocity on the behavior of temperature is not significant; expect the values of temperature and decays rates, which differ for the different cutting speeds. In this case, increasing cutting speed reduces the peak value of temperature. It should be noted that the maximum temperature is 1600 K at the cutting edge and location $x = -2.75$ mm; $y = 75$ mm, and $z = 0$ mm is slightly away from the edge ($x = -2.0$ mm, $y = 7.5$ mm, and $z = 0$ mm). Consequently, changing in the peak temperature reveals that conduction heating on the region considered is less for the high cutting speed while lowering the peak value of temperature. This is also true for the temperature gradient along the y-axis, in particular in the neighborhood of the laser peak power intensity. In this case, increasing cutting speed lowers the temperature gradient along the y-axis in this region. In the case of location $x = -2.75$ mm, $y = -7.5$ mm, and $z = 0$ mm, temperature remains low for all the cutting velocities. This is because of the completion of the cutting process. The conduction cooling in the region $x = -2.75$ mm, $y = -7.5$ mm, and $z = 0$ mm results in the attainment of low temperature in this region. It should be noted that the time shown for each laser cutting speed indicates the completion of the cutting process for particular speed at this location, i.e., the cutting of the rectangular tailored blank ends at point A (Fig. 1).
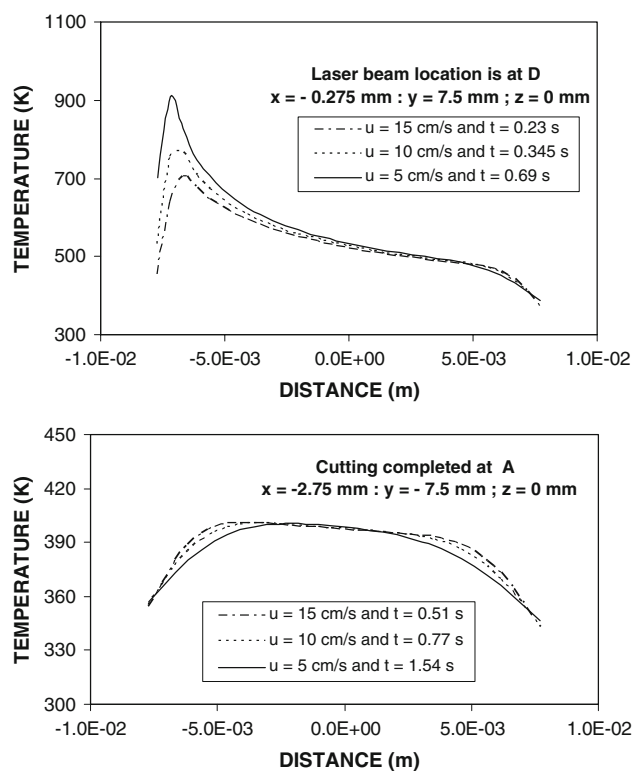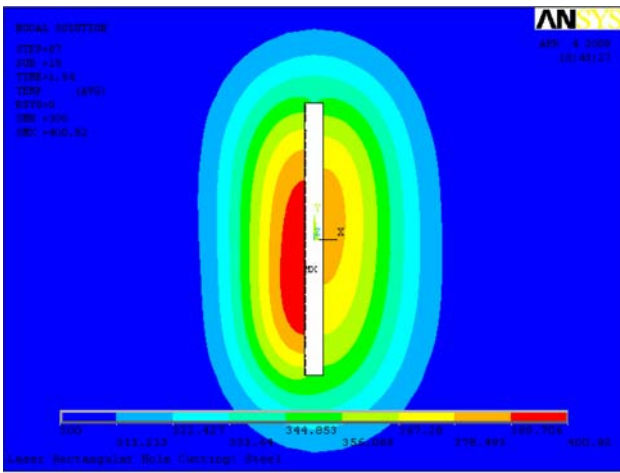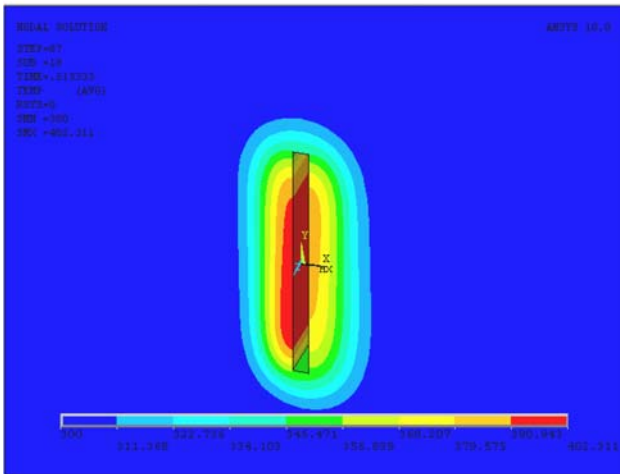

Fig. 2 Temperature distribution along the y-axis for different cutting speeds

Table 2 Laser cutting parameters

Feed rate, m/s	Power, W	Frequency, Hz	Nozzle gap, mm	Nozzle diameter, mm	Focus diameter, mm	N$_2$ pressure, kPa
0.05, 0.1, 0.15	1800	300	1.5	1.5	0.3	500

Cutting speed = 5 cm/s

Cutting speed = 15 cm/s

Fig. 3 The plane view of temperature contours after laser cutting is completed

Fig. 4 Von Mises stress distribution along the y-axis for different cutting speeds

Figure 4 shows von Mises stress along the y-axis for three laser cutting speeds at the same locations shown in Fig. 2 while Fig. 5 shows the plane view of von Mises stress in the cutting sections. Von Mises stress reaches the maximum in the close region of the maximum temperature (Fig. 2). However, the location of the maximum von Mises stress is further away from the location of the maximum temperature. It should be noted that the temperature gradient in the region next to the maximum temperature is the highest along the y-axis resulting in high stress levels in this region. Consequently, von Mises stress becomes high. Moreover, as the temperature gradient changes from sharp to gradual decay along the y-axis, von Mises stress reduces to its minimum. This may be associated with the thermal strain developed in this region, which is low due to compressive and tensile stresses merge in this region. As the distance along the y-axis increases further, von Mises stress increases despite the fact that the temperature gradient change is gradual in this region. This is because of the thermal strain, which increases along the y-axis. The influence of cutting speed on von Mises stress is considerable; in which case, low cutting speed results in high level of von Mises stress. This is particularly true at the distance away from the laser beam
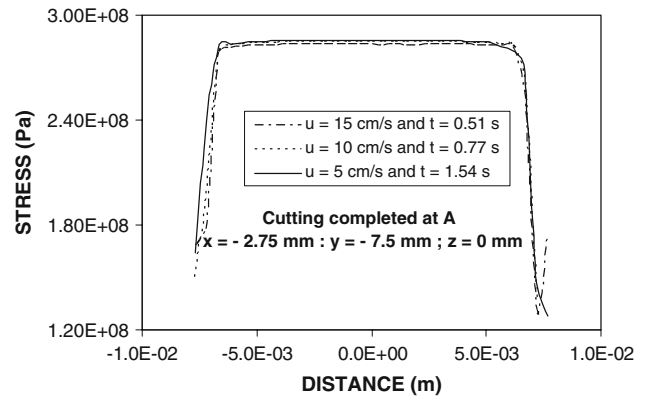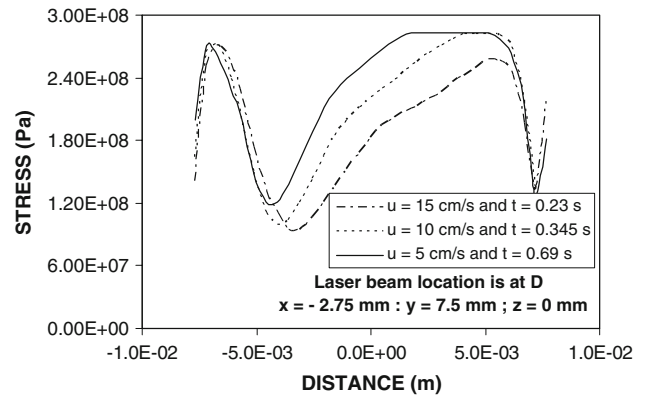
intensity ($y \geq -2.0$ mm). This is because of the high temperature gradient developed along the y-axis for the low cutting speed ($u \leq 10$ cm/s). In the case of von Mises stress at location $x = -2.5$ mm; $y = 7.5$ mm, and $z = 0$ mm, it increases sharply and remains high. Since temperature at this location is low due to cooling, the stress level represents the residual stress in this region. Consequently, the residual stress levels remain high along the y-axis which is less than the yield limit of the substrate material, i.e., it is in the order of 280 MPa. The influence of cutting speed on the residual stress is not significant. In this case, the cooling rate of the substrate material does not alter significantly along the y-axis resulting in almost the same magnitude of the residual stress for all cutting speeds.

Figure 6 shows temporal variation of temperature at the location when laser beam is at point "D" (Fig. 1) for three laser scanning speeds. The maximum temperature occurs at different times for different speeds in location "D". This is because of the laser beam intensity reaching at point "D" differs for different cutting speeds. The temporal decay rate of temperature from its maximum changes with time; in which case, the decay rate becomes high immediately after reaching the maximum temperature. As the time progresses further, the decay rate becomes gradual. However, the decay rate changes with the cutting speed particularly at the time period immediately after the maximum temperature. Temperature decay rate is higher for the high cutting speed than that corresponding to the low cutting speed (5 cm/s). The maximum temperature remains the same for all the speeds considered in the simulations. This is
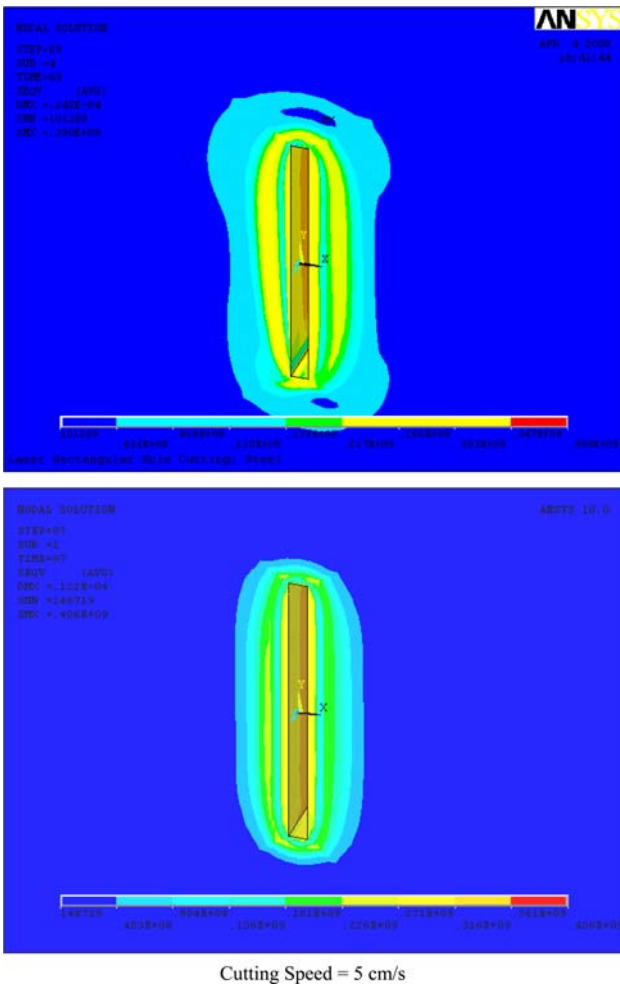
Cutting Speed = 5 cm/s

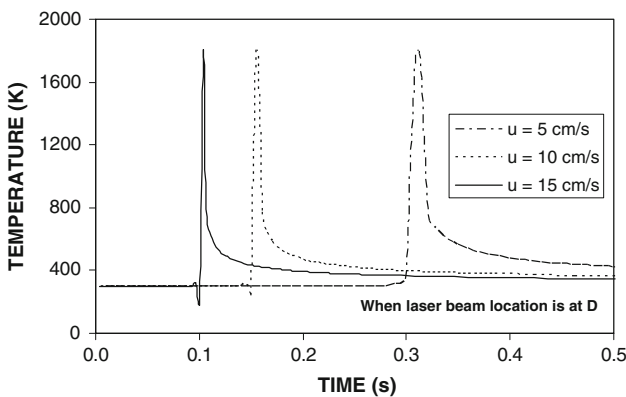**Fig. 5** The plane view of von Mises contours after laser cutting is completed

Fig. 6 Temporal variation of temperature for three cutting speeds

because of the resulting maximum temperature in the substrate material, which remains the same for all the simulation conditions, i.e., the maximum temperature at the cut surface between the liquid metal and solid remains at the melting temperature of the substrate material.

Since the variation of von Mises stress is almost the same at each corner of the rectangular cut, only one corner is discussed
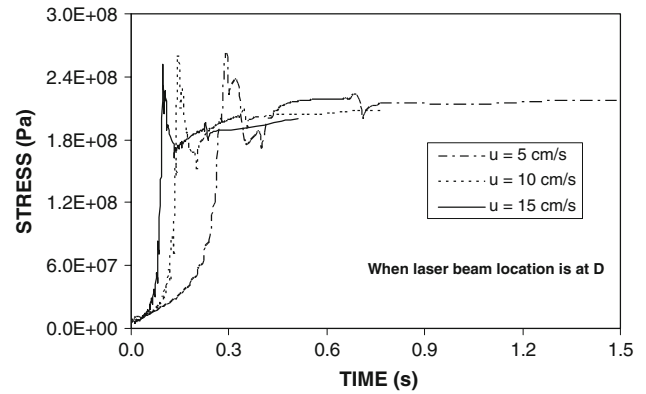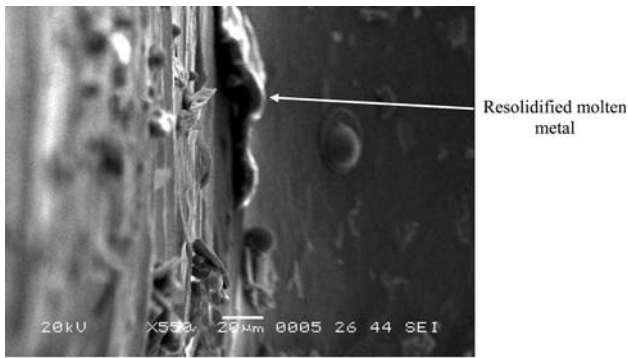

Fig. 7 Temporal variation of von Mises stress for three cutting speeds

Table 3 Predictions and measured values of residual stresses in the region around the location D along the cut edge
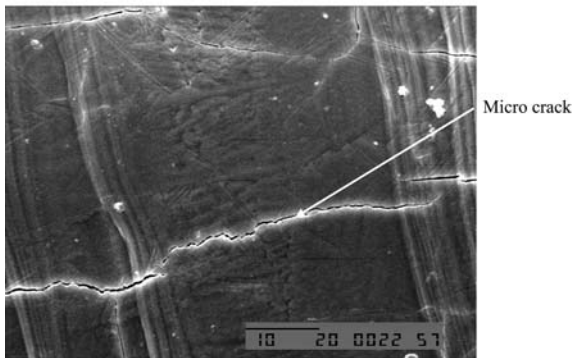
Speed, m/s	Residual stress predictions, MPa	Residual stress experiment, MPa
0.05	220	230
0.1	200	210
0.15	180	170

in Fig. 7, in which temporal variation of von Mises stress for different laser cutting speeds at the same location of Fig. 6 is shown, i.e., location "D." Von Mises stress rises rapidly to reach its maximum for the high cutting speed (15 cm/s). This is because of the rapid decay of temperature during the time period immediately after reaching the maximum temperature. Moreover, the rise of stress is relatively lower for the low cutting speed than that corresponding to the high cutting speed. The decay of the stress levels from its maxima is gradual due to gradual decrease of temperature during this duration. Once the low temperature is attained after cooling, the stress level remains almost steady with progressing time. This situation is true for all the cutting speeds. This indicates that the stress formed after the cooling period becomes a residual stress at location "D" in the cutting section. The magnitude of residual stress remains almost the same for all the cutting speeds. The residual stress developed is in the order of 180 MPa, which is less than the elastic limit of the substrate material. Consequently, the crack formation in the corner of the rectangular cut is not probable due to low stress levels developed in this region. Table 3 gives the residual stress predicted from the present simulation and measured using the XRD technique. It can be observed that the predictions agreed with the experimental data for all cutting velocities considered in the present study. However, the influence of the cutting speed on the residual stress levels is negligibly small.

Figure 8 shows optical and SEM micrographs of the cut sections for the different cutting speeds. The depth of strias increases slightly with reducing cutting speed. However, the stria length is almost the same for all the cutting speeds. It should be noted that the side ways burning and thermal erosion are responsible for the formation of deep strias. Consequently, at low cutting speeds, the rate of energy transfer to the cut

Resolidified molten metal

Cutting speed = 5 cm/s

Micro crack

Cutting speed = 15 cm/s

Fig. 8 SEM micrographs of the cutting surfaces

Partial formation of cementite

Fig. 10 SEM micrograph of cutting edge cross section in the region of heat-affected zone
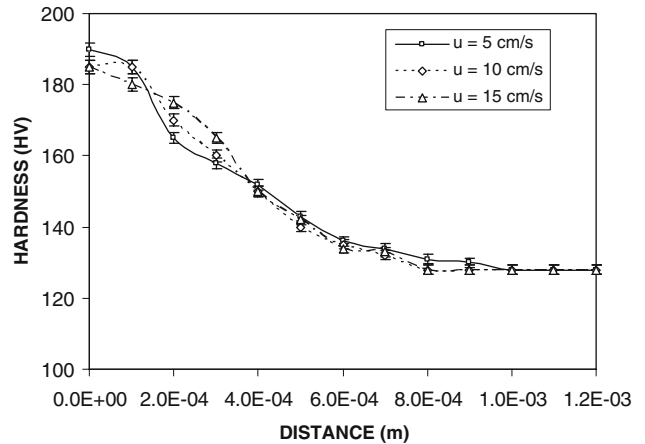
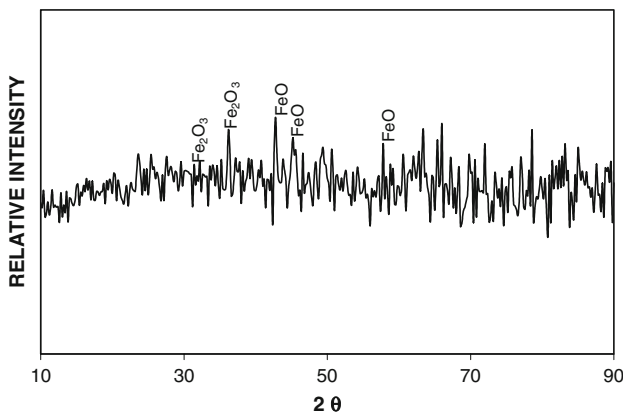**Fig. 11** Microhardness distribution across the cutting edge

Fig. 9 XRD result for the cut edge

section from the laser heat source increases, which in turn enhances the thermal erosion along the cut surfaces. The rapid solidification of thin molten layer on the solid at the cut surface results in fine and shallow surface cracks. Moreover, the contribution of oxygen diffusion in the molten zone contributes the fine cracking at the surface onset of the rapid solidification. The existing of oxide compounds at the surface is also evident from the XRD plot (Fig. 9). The fine surface cracking is more pronounced at high cutting speeds due to the rapid temperature decay in the surface region. However, some liquid buildup at the surface is observed at the bottom region of the cutting surface. The small molten buildup and later solidification is the indication of the high rate of the thermal erosion. In this case, thickening of the molten layer increases the shear stress against the assisting gas inertia force. The surface tension, then, rounds
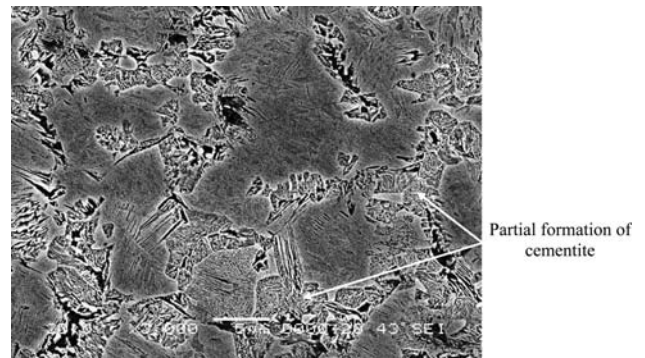
the molten buildup in this region. Moreover, no dross attachment is observed at the bottom region of the cut surface. The grain coarsening in the heat-affected zone is evident from the micrograph (Fig. 10). In addition, nucleation of pearlite results in partial formation of cementite lamellae structure in the neighborhood of the re-solidified region. However, the grains mainly consist of ferrite and fine pearlite structure. Figure 11 shows microhardness results across the cutting surface cross section. It is evident that hardness attains almost 60% of the base material hardness in the resolidified region and reduces sharply in the heat-affected zone. As the distance increases away from the cutting surface hardness reduces to the base material hardness indicating the narrow heat-affected zone. The influence of the cutting speed on the hardness is not significant, provided that the depth of heat-affected zone is slightly extended for the low speed. This is attributed to the heat conduction from the cutting surface during the heating and cooling periods of the cutting process.

6. Conclusions

Laser cutting of rectangular blank into mild steel sheet is considered and temperature as well as thermal stress fields are predicted using the FEM. The influence of laser cutting speed on temperature and stress fields is examined while the residual stress developed in the cutting region is measured using the

XRD technique. The morphological and metallurgical changes in the cutting region are examined using the SEM and XRD. It is found that the maximum temperature attains slightly higher values along the y-axis for the low cutting speed (5 cm/s) than those correspond to the high cutting speeds. This is in turn, modifies the temperature gradient slightly along the y-axis. As a consequence of this, von Mises stress distribution along the y-axis changes with the cutting speed such that von Mises stress attains higher values for high cutting speeds than the low cutting speed. Von Mises stress reduces to a local minimum along the y-axis for all the cutting speeds because of the change in the temperature gradient in this region. The temporal behavior of von Mises stress reveals that the rate of increase in von Mises stress is higher for the high cutting speed than the low cutting speeds (10 and 5 cm/s). However, the magnitude of residual stress remains the same in the corner of rectangular cut for all the cutting speeds. The residual stress developed in the region of the cut edges agree with the experimental data for all cutting speeds employed in the present study. The depth of stria is slightly larger for low cutting speed then the high cutting speed. The thermal erosion is responsible for this enlargement. The scattered fine surface cracks are observed on the cutting surface. The oxygen diffusion in this region contributes to the crack formation. The hardness profile across the cutting cross section shows that the heat-affected zone is narrow for all the cutting speeds, except it extends slightly for the low cutting speed. The maximum hardness occurs in the resolidified zone in the vicinity of the cutting surface and the maximum hardness reaches almost 60% of the base material hardness in this region.

Acknowledgment

References

1. K. Li and P. Sheng, Plane Stress Model for Fracture of Ceramics During Laser Cutting, *Int. J. Mach. Tools Manuf.*, 1995, **35**(11), p 1493–1506

2. A. Kotousov and J.W.H. Price, Stress Intensity Factor for Semi-Infinite Crack Formed by Moving Thermal Source, *Int. J. Fract.*, 1998, **90**(3), p L39–42

3. M.F. Modest and T.M. Mallison, Transient Elastic Thermal Stress Development During Laser Scribing of Ceramics, *J. Heat Trans.*, 2001, **123**(1), p 171–177

4. G. Hardjadinata and C.C. Doumanidis, Rapid Prototyping by Laser Foil Bonding and Cutting: Thermomechanical Modeling and Process Optimization, *J. Manuf. Process.*, 2001, **3**, p 108–119

5. C.H. Tsai and C.J. Chen, Formation of the Breaking Surface of Alumina in Laser Cutting with a Controlled Fracture Technique, *Proc. Inst. Mech. Eng. B J. Eng. Manuf.*, 2003, **217**(4), p 489–497

6. S.H. Lee and S. Ahn, A Probabilistic Model for Crack Formation in Laser Cutting of Ceramics, *JSME Int. J. C Mech. Syst. Mach. Element Manuf.*, 2003, **46**(4), p 1591–1597

7. N. Paterson, A. Tawn, K. Williams, and A.D. Nurse, On the Numerical Modeling of Laser Shearing of Glass Sheets Used to Optimize Production Methods, *Proc. Inst. Mech. Eng. C J. Mech. Eng. Sci.*, 2004, **218**, p 1–11

8. R. Akarapu, B.Q. Li, and A. Segall, A Thermal Stress and Failure Model for Laser Cutting and Forming Operations, *J. Fail. Anal. Prevent.*, 2004, **4**(5), p 51–62

9. B.S. Yilbas, A.F.M. Arif, C. Karatas, and M. Ahsan, Cemented Carbide Tool: Laser Processing and Thermal Stress Analysis, *Appl. Surf. Sci.*, 2007, **253**(12), p 5544–5552

10. G. Germain, P.D. Santo, J.L. Lebrun, D. Bellett, and P. Robert, Thermal and Thermo-Mechanical Simulation of Laser Assisted Machining, *Proceeding of 10th EASFORM Conference on Material Forming*, Zaragoza, Spain, 2007, p 1251–1256

11. B.S. Yilbas and N. Al-Ageeli, Formulation of Laser Induced Thermal Stresses: Stress Boundary at the Surface, *Proc. Inst. Mech. Eng. C J. Mech. Eng. Sci.*, 2003, **217**, p 423–434

12. B.S. Yilbas and N. Al-Ageeli, Thermal Stresses due to Time Exponentially Decaying Laser Pulse: Elasto Plastic Wave Propagation, *Int. J. Mech. Sci.*, 2004, **46**, p 57–80

13. B.S. Yilbas, N. Al-Ageeli, and M. Kalyon, Laser Induced Thermal Stresses in Solids: Exponentially Time Decaying Pulse Case, *Laser Eng.*, 2004, **14**(1), p 81–101

14. B.S. Yilbas and N. Al-Ageeli, Thermal Stress Development Due to Laser Step Input Pulse Intensity Heating, *J. Therm. Stress.*, 2006, **29**(8), p 721–751

15. A.F.M. Arif and B.S. Yilbas, Thermal Stress Developed During Laser Cutting Process: Consideration of Different Materials, *Int. J. Adv. Manuf. Technol.*, 2008, **37**, p 84–92

16. T.C. Totemeier and R.N. Wright, Residual Stress Determination in Thermally Sprayed Coatings—A Comparison of Curvature Models and X-Ray Techniques, *Surface Coat. Technol.*, 2006, **200**(12–13), p 3962–3995